BEM Simulation and Experimental Test of a FML Full Scale Aeronautic Panel Undergoing Biaxial Static and Fatigue Load

E. Armentani[1], V. Ascione[2], R. Citarella[3], R. Sepe[4]

[1] Dept. of Materials Engineering and Production, University of Naples, P.le V. Tecchio, 80 – 80125 Naples, Italy; E-mail: enrico.armentani@unina.it.
[2] Alenia Aeronautica, Viale dell'Aeronautica, 80038 Pomigliano d'Arco, Naples, Italy; E-mail: vascione@alenia.it.
[3] Dept. of Mechanical Engineering, University of Salerno, Via Ponte Don Melillo, Fisciano (SA), Italy; E-mail: rcitarella@unisa.it.
[4] Dept. of Materials Engineering and Production, University of Naples, P.le V. Tecchio, 80 – 80125 Naples, Italy; E-mail: raffsepe@unina.it.

ABSTRACT. *This paper concerns the numerical and experimental characterization of the static and fatigue strength of a flat stiffened panel, designed as a fiber metal laminates (FML) and made of Aluminum alloy and Fiber Glass FRP. The panel is full scale and was tested under both static and fatigue biaxial loads, applied by means of an in house designed and built multi-axial fatigue machine. The static test is simulated by the Boundary Element Method (BEM) in a two-dimensional approach (only allowance for membrane stresses). The strain gauge outcomes are compared with corresponding numerical results, getting a satisfactory correlation. After the static test, an initial notch is created in the panel and the aforementioned biaxial fatigue load is applied, causing a crack initiation and propagation; the related experimental initiation times and crack growth rates are provided.*

INTRODUCTION

To achieve high-performance aircraft structures new tailored and cost-effective materials are continuosly designed and tested. Nowadays the Fibres Metal Laminate (FML) technology is optimised for fatigue and damage tolerance properties, that is one of the reasons for its application in the upper shells of the A380 fusolage, but a balanced performance in terms of static properties is also obtainable, leading to a significant reduction in terms of weight and operating cost.

This paper concerns an investigation on the application of innovative materials obtained by the use of improved lamina and fibre reinforcements (FML) to panels of a typical wide body fuselage section. The requirements for a numerical model, based on the Boundary Element Method (BEM) [1], capable of assessing the static behaviour of selected details made of FML (Glare is an example of such hybrid material with considerably good damage tolerance properties), are provided. Moreover a multiaxial

fatigue experimental test was performed: a crack initiation from a preexhisting notch and consequent propagation is described, providing the initiation time and growth rates.

The forward side panel of the DIALFAST fuselage has been considered (DIALFAST is the name of a European project in which such panel was developed and analysed).

TEST ARTICLE DESCRIPTION AND EXPERIMENTAL TEST

A Metal Barrel, which is representative of Airbus A330/340 fuselage section 16 (Figure 1a), has been considered as a reference structure in order to define the design solution for a stiffened panel made of innovative FML. The panel consists of three bays joined together by butt-straps and z-shape stringer coupling; windows cut-outs are included in the structure (Figure 1b). The stringer pitch and the frame pitch are equal to, respectively, 172.3 mm and 533 mm. The panel is made of two parts: an upper and a lower panel, joined by a lap joint at the stringer N.6 (Figure 2). The frames are applied on both panel sides to minimize the secondary bending effects. In detail the panel consists of the following parts: FML skin, FML stringers bonded to the skin, metallic frames and cleats (Al 2024-T3 clad sheet) riveted to the skin, metallic window frames (7075 – T651 Hand forming) bonded to the skin. The FML skin (3/2-0.3mm-0°/90°) and stringer (3/2-0.3 mm-0°/0°) layups and the used materials are shown in Tables 1a-b.

The tested panel has been instrumented by strain gages, that are located on both sides in order to provide information about the secondary bending relevance. Specifically ten strain rosettes with three legs disposed at 0°-45°-90° (type CEA-13-250UR-350) and 8 strain gages (type CEA-13-250UW-350) were installed on the specimen. The strain gages were bonded on both sides of the panel (side A and B) by a two-component epoxy adhesive in order to assure good performance in precence of large strains. The layout of strain rosettes and strain gages on the side A is shown in Figure 2; whereas the positioning coordinates (x, y) of strain gages and rosettes are reported in Table 2.

The tested specimen has been subjected to a load test (load values are taken from previous studies developed within DIALFAST project) by the multiaxial test machine shown in Figure 1b [2]. Eight clamps on each side of the panel transfer the load by 4 properly shaped pins, either by shear or by pin clamping friction. The 8 clamps are linked by a lever system to their respective traction load-applying cylinders. To apply the external loads without causing damages on the panel borders, six aluminium plates are joined to the panel. This loading system allows independent deformations along different directions on the skin plane. The same set of grips applies both normal and shear loads; a balancing system assures that the normal load is uniformly distributed on the edge. The boundary conditions are “simply supported edges” constraints, i.e. the in-plane displacements are allowed, whereas the out-of-plane displacements at the panel edges are constrained by means of a rolling bearing system.

Loads are applied along two orthogonal directions by four hydraulic cylinders. It would be also possible to apply a static load in one direction and a fatigue load in the other.

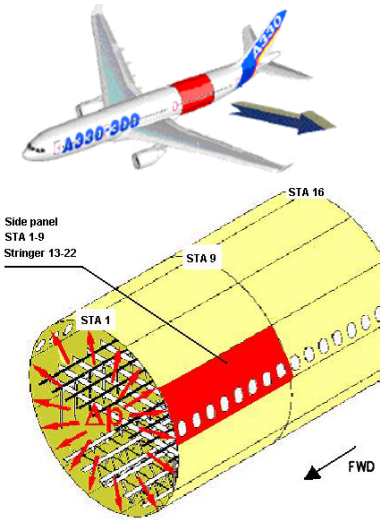

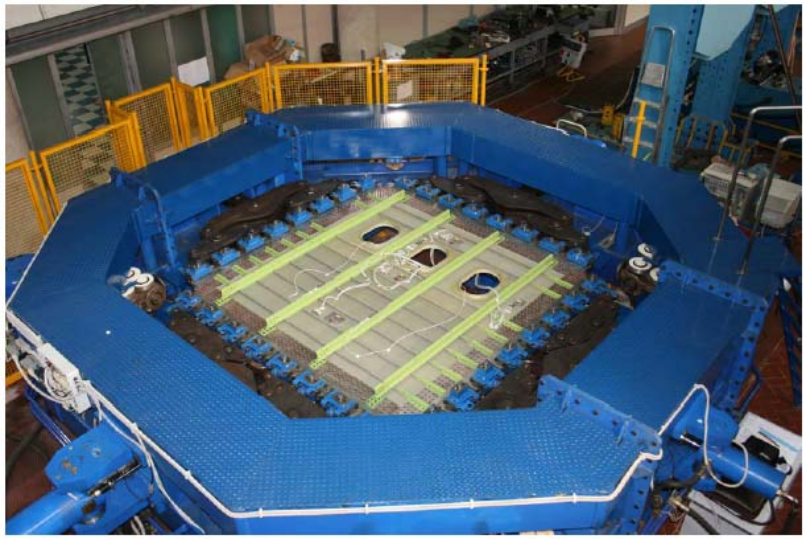

a) b)

Figures 1a-b DIALFAST barrel and tested panel loaded by the multi-axial fatigue machine.

Table 1a-b Skin and stringer lay-up and adopted material.

PLY	MATL	SKIN ORIENT.	STRINGER ORIE.	THK [mm]
P1	LAMINA	N/A	N/A	0.3
P2	F/G	0°	0°	0.125
P3	F/G	90°	0°	0.125
P1	LAMINA	N/A	N/A	0.3
P3	F/G	90°	0°	0.125
P2	F/G	0°	0°	0.125
P1	LAMINA	N/A	N/A	0.3

Component	Material
Lamina Skin	Alloy 7475 – T761
FG Prepreg	FG FM 94-22% - S2 GLASS – 187-460
Frame	Alloy 2024 – T3 CLAD
Shear cleats	Alloy 2024 – T3 CLAD
Window frame	Alloy 7075 – T651
Plates	Alloy 6056 – T4

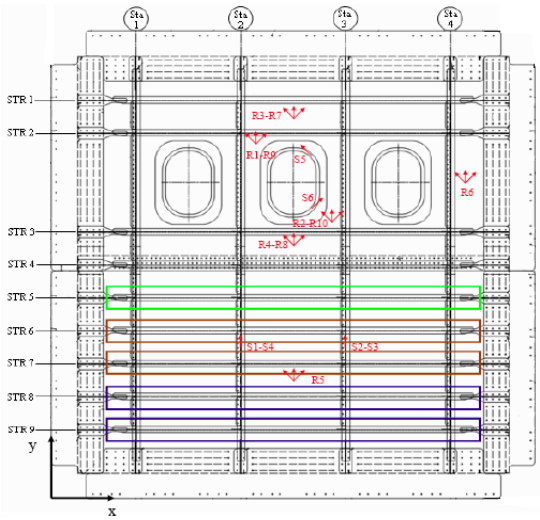

Figure 2 Strain gage and rosette configuration on side A.

Table 2 Strain gages and rosette positions on sides A and B of the panel.

Side A	R1	R2	R3	R4	R5	R6	S1	S2
x [mm]	1017	1430	1220	1220	1220	2104	970	1500
y [mm]	1835	1475	2010	1320	631	1655	787	787
Side B	R7	R8	R9	R10	S3	S4	S5	S6
x [mm]	1220	1220	1017	1430	1500	970	1332	1332
y [mm]	2010	1320	1835	1475	787	787	1767	1543

Four types of tests have been carried out:

- T1: Bi-axial static test - P_x = 125 kN - P_y = 250 kN, with loads applied in load control by a ramp of 0.5 kN/sec in x direction and of 1 kN/sec in y direction;
- T2: Mono-axial static test - P_y = 250 kN, with loads applied in load control with a ramp of 1 kN/sec;
- T3: Mono-axial static test - P_x = 125 kN, with loads applied in load control with a ramp of 0.5 kN/sec;
- T4 Bi-axial fatigue test- P_{xmax} = 125 kN - P_{ymax} = 250 kN, with loads applied by a frequency of 1 Hz in both direction and ratio R = 0.1.

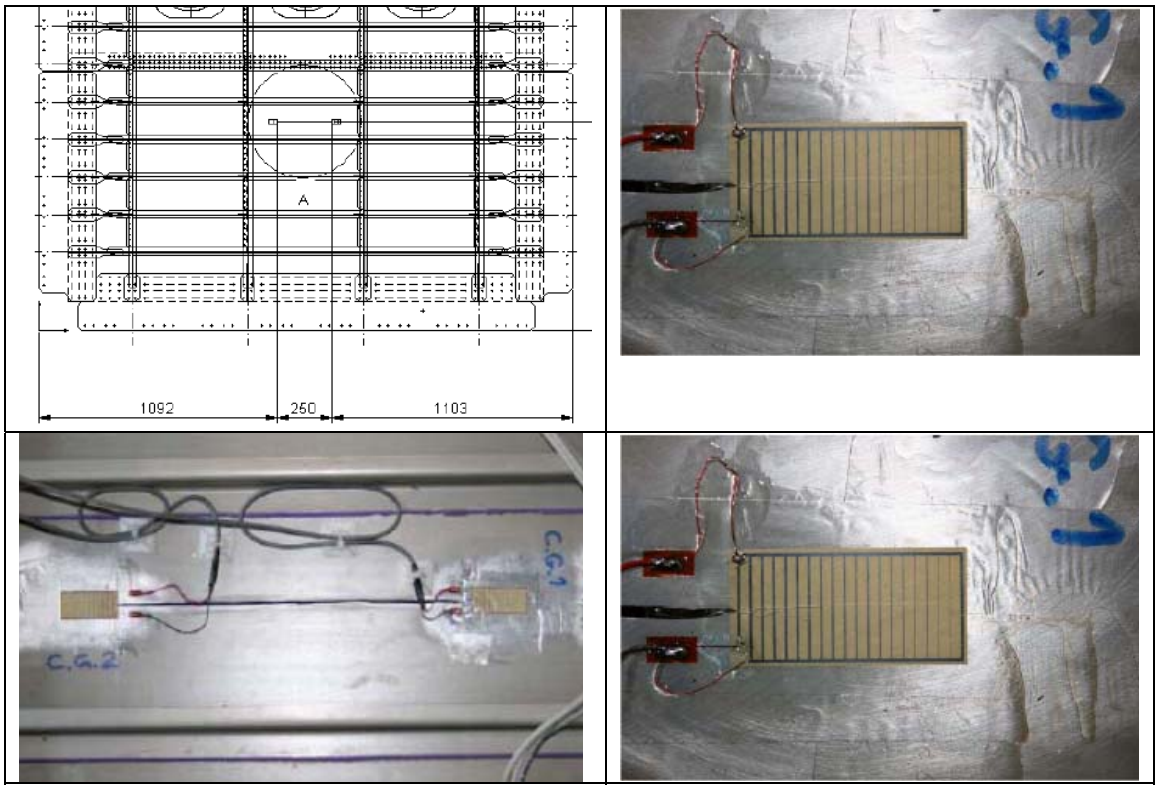

Figure 3 Notch and crack gage positions: initial (left) and final (right) configurations.

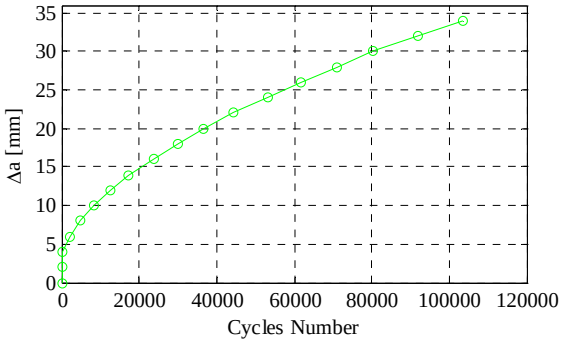

Figure 4 Δa-N curve by the sensor C.G.1.

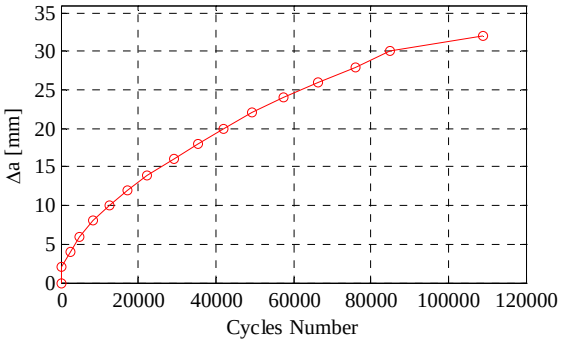

Figure 5 Δa-N curve by the sensor C.G.2.

Before starting the fatigue test a notch was saw cut in order to localise in advance the crack initiation, whereas the crack propagation was monitored by crack gauge sensors (TK09-CPC03-003/DP). The position of the initial notch and crack gages are shown in Figure 3, together with a close-up of the propagated crack. Propagation curves related to test T4 are shown in Figures 4 and 5. When the crack reached an overall advance of nearly 70 mm the fatigue test T4 was stopped and a residual strength test was realised with a static biaxial load reaching the values P_{xmax} = 250 kN and P_{ymax} = 500 kN. Such final load (no further increase was allowed due to actuators limitations) was not sufficient to produce any crack instability, nor to produce any stable crack advance.

BEM MODEL AND NUMERICAL-EXPERIMENTAL CORRELATION

The BEM model is two dimensional and the underlying modelling approach is described in [3-5]: each single component (skin, stringers, frames and shear cleats) is explicitly modelled with allowance for its in plane stiffness. The mesh is based on nearly ten thousands linear elements. In Figures 6 and 7 the BEM model and the maximum principal stresses [MPa] are shown for the three loading configurations analysed (T1-3). In Tables 3 and 5 the numerical strains provided along the strain gages directions are compared with the corresponding experimental data. The comparison with the numerical membrane strains is prevented when the experimental strains on strain gages, located in the same position and direction but on the opposite sides of the panel, are substantially different: this shows the presence of local bulging effects and the consequent need for a more complex modelling. Moreover the comparison with reference to the strain gages S1-S6 is only provided when the loading is applied along the frame direction because the secondary bending is minimised.

The rivet compliance is calculated with the Mac Donnell Douglas formula:

$$C = \frac{5}{D \cdot E_3} + 0{,}8\left(\frac{1}{t_1 \cdot E_1} + \frac{1}{t_2 \cdot E_2}\right)$$

where: t_i=thickness of connected panels, $E_{1,2}$= Young modulus of the panels, $E_{3=}$ Young modulus of rivet, D= rivet diameter.

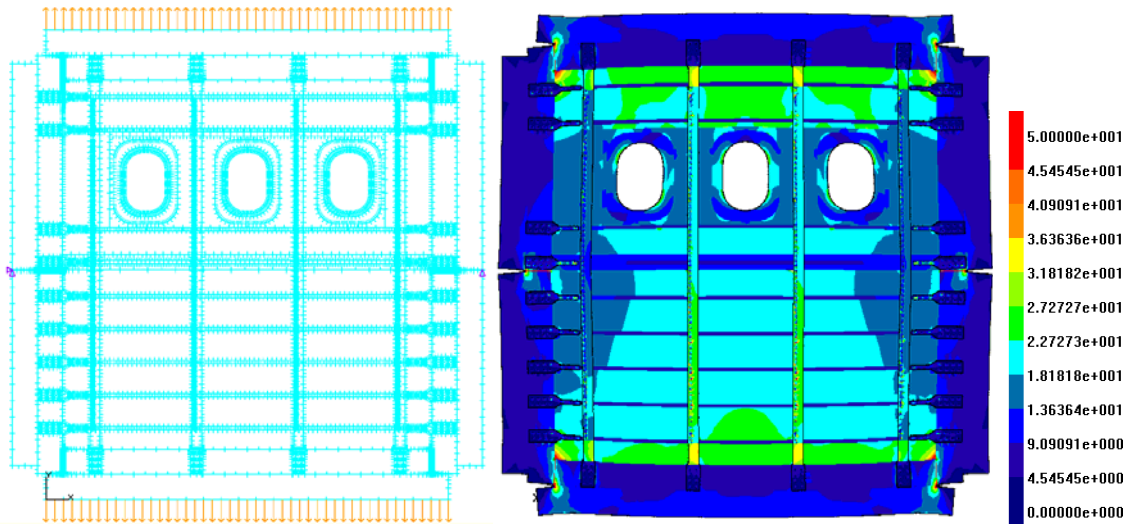

Figure 6 BEM model and max. principal stresses (MPa) with load configuration T3.

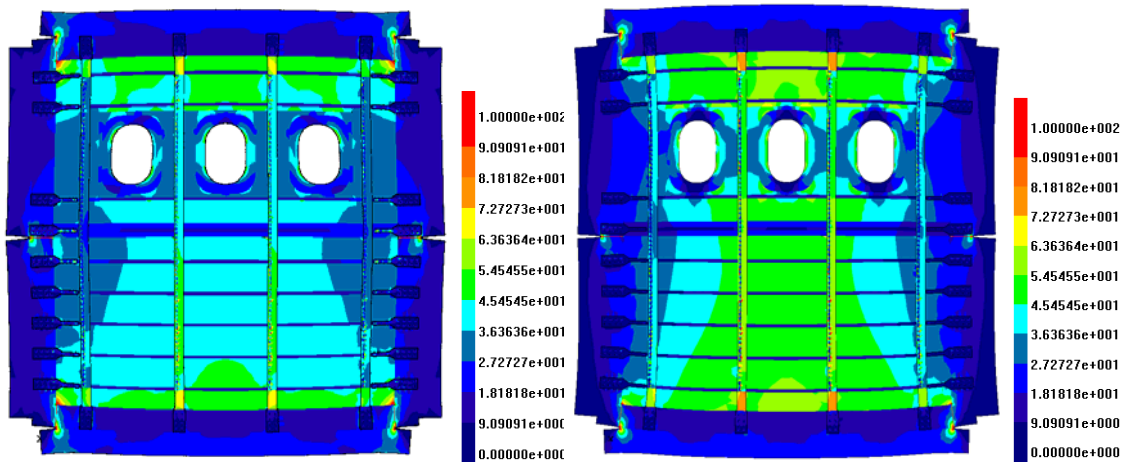

Figure 7 BEM deformed plot with max principal stresses (MPa) with load configurations T1 (left) and T2 (right).

CONCLUSIONS

With reference to the static test, the correlation between numerical and experimental results is judged satisfactory, especially considering the simplicity of the adopted BEM approach (the modeling and meshing process is straightforward) and the reduced computational effort.
The obtained crack growth rates turn out to be decreasing with crack advances, showing the optimal damage tolerance properties of the used material. Unfortunately the maximum static applicable loads were not sufficient to complete the residual strength test but anyway provided a minimum safety threshold.

Table 3 Numerical and experimental correlection for load configuration T1

Single or coupled strain gages	Biaxial load (T1)				
	BEM strain (a)	Experimental strain			Error(%)=(a-b)*100/a
		Side A	Side B	Average strain (b)	
R1-1/9-3	352	375	422	398.5	-13.2
R1-2/9-2	572	593	624	608.5	-6.4
R1-3/9-1	306	378	375	376.5	-23.0
R2-1/10-3	287	360	244	302	local bulging
R2-2/10-2	507	584	810	697	local bulging
R2-3/10-1	428	414	254	334	local bulging
R3-1/7-3	511	508	513	510.5	0.1
R3-2/7-2	932	811	821	816	12.4
R3-3/7-1	496	486	503	494.5	0.3
R4-1/8-3	480	510	461	485.5	-1.1
R4-2/8-2	742	777	645	711	4.2
R4-3/8-1	480	525	502	513.5	-7.0
R5-1	462	475	-	475	-2.8
R5-2	836	805	-	805	3.7
R5-3	464	478	-	478	-3.0

Table 4 Numerical and experimental correlection for load configuration T3

Single or coupled strain gages	Uniaxial load along stringer direction (T3)				
	BEM strain (a)	Experimental strain			Error (%)= (a-b)*100/a
		Side A	Side B	Average strain (b)	
R1-1/9-3	159	230	105	168	local bulging
R1-2/9-2	-206	-214	-256	-235	-14.1
R1-3/9-1	72	70	75	73	-1.2
R2-1/10-3	197	289	117	203	local bulging
R2-2/10-2	-272	-258	-299	-278	-2.4
R2-3/10-1	122	96	131	114	local bulging
R3-1/7-3	99	122	114	118	-19.0
R3-2/7-2	-55	-51	-82	-66	local bulging
R3-3/7-1	105	106	94	100	4.5
R4-1/8-3	167	192	210	201	-20.3
R4-2/8-2	-150	-129	-159	-144	3.9
R4-3/8-1	160	158	174	166	-3.6
R5-1	121	129	-	129	-6.7
R5-2	-147	-145	-	-145	1.6
R5-3	121	142	-	142	-17.0

Table 5 Numerical and experimental correlection for load configuration T2

Single or coupled strain gages	Uniaxial load along frame direction (T2)				
	BEM strain (a)	experimental strain			Error (%)= (a-b)*100/a
		Side A	Side B	Average strain (b)	
R1-1/9-3	141	157	329	243	local bulging
R1-2/9-2	786	807	884	846	-7.6
R1-3/9-1	278	285	308	297	-6.7
R2-1/10-3	84	82	244	163	local bulging
R2-2/10-2	790	840	810	825	-4.4
R2-3/10-1	303	316	254	285	5.9
R3-1/7-3	409	409	414	412	-0.6
R3-2/7-2	984	893	903	898	8.7
R3-3/7-1	386	370	388	379	1.8
R4-1/8-3	308	344	285	315	-2.1
R4-2//8-2	895	928	789	859	4.1
R4-3/8-1	315	368	329	349	-10.6
R5-1	337	358	-	358	-6.2
R5-2	988	987	-	987	0.1
R5-3	340	356	-	356	-4.7
S1	851	915	-	915	-7.5
S2	847	1001	-	1001	-18.2
S3	811	850	-	850	-4.8
S4	813	788	-	788	3.1
S5	547	613	-	613	-12.1
S6	517	639	-	639	-23.6

REFERENCES

1. Aliabadi M. H. (2002). In: *The Boundary Element Method*, vol. 2, John Wiley and Sons, LTD, England.
2. Armentani E., Caputo F., Esposito R., Godono G., A new three loading axes machine for static and fatigue tests, Proceedings of the Sixth International Conference on Biaxial/Multiaxial Fatigue & Fracture (6th ICBMFF), Lisboa, Portugal, June 25-28, 2001, Vol. 1, pp. 323-330.
3. Armentani E., Citarella R. (2006) DBEM and FEM analysis on non-linear multiple crack propagation in an aeronautic doubler-skin assembly, *International Journal of Fatigue*, 28**,** 598–608.
4. Citarella R., Lepore M., Apicella A., Calì C. (2007) DBEM Crack Growth Simulation for a Riveted Aeronautic Reinforcement under Non-linear Contact Conditions, *Key Engineering Materials*, 348-349, 593-596.
5. Citarella R., (2009) Non Linear MSD crack growth by DBEM for a riveted aeronautic reinforcement, *Advances in Engineering Software* 40**,** 253–259.